JOURNAL OF COMPUTATIONAL PHYSICS **138,** 153–170 (1997)
ARTICLE NO. CP975821

Bound States of a One-Band Model for 3D Periodic Medium

Alexander Figotin and Igor Khalfin

Department of Mathematics, University of North Carolina at Charlotte, Charlotte, North Carolina 28223
E-mail: figotin@uncc.edu

Received November 15, 1996

We consider the bound states generated by impurities in a periodic three dimensional medium. The computations of eigenstates and eigenfunctions for a one-band model of the medium are carried out. Using numerical evaluation of the Green's function for bound eigenmode representations we achieve high accuracy in the computation of the eigenmodes and eigenstates for a variety of defects. For appropriately adjusted models these computations can be useful for numerical estimates of the minimal configuration of defects capable of introducing a bound state in a gap, as well as estimating the rate of the exponential decay of the bound state.

Key Words: periodic Schrödinger operator; propagation of electromagnetic and acoustic waves; band gap structure of the spectrum.

1. INTRODUCTION

This work is motivated by the recent interest and new developments in the localization of classical electromagnetic and acoustic waves [1–3]. Our focus here will be on the properties of localized or bound states due to a single defect in a three-dimensional periodic medium. It follows from the theory of solids that if the spectrum of periodic Schrödinger operator has a gap and a defect is introduced, then an exponentially localized state, called *bound*, *impurity*, *or defect state*, may arise [4]. A similar statement holds also for the classical electromagnetic and acoustic waves [1, 2, 5, 6]. The quantitative study of properties of bound states in three-dimensional space is a challenging problem. The Schrödinger equation with a three-dimensional square well potential is one of a few examples, where the bound states are studied in detail analytically because of the spherical symmetry of the potential which allows the reduction of three-dimensional PDE to a one-dimensional ODE

0021-9991/97 $25.00

[7]. Another example of a model that can be analyzed analytically is the Schrödinger equation with a finite number of point defects [8]. But many interesting and important problems in *three dimensions* for bound states generated by one or more defects are still beyond pure analytical methods. To list a few, we may mention the following problems: (i) the number of bound eigenstates in a given spectral gap; (ii) the value of the threshold "strength" of the defect sufficient to generate a bound state and the behavior of the associated eigenmode when the defect is near that threshold "strength"; (iii) the value of the radius of localization for a given bound eigenmode; (iv) the properties of bound eigenmodes for two or more separated defects.

To address the above problems we introduce and consider a one-band model associated with the underlying periodic medium. Namely, we single out the band which is the closest to the bound state of interest. One can show that the one-band model is unitarily equivalent to a 3D lattice model. A typical and, probably, the simplest example of the one-band model of a periodic medium is the 3D lattice Laplacian H_0 which will be our basic example. Then we introduce a defect in the form of the lattice potential $V(x)$ (x runs the sites of the 3D lattice) which vanishes everywhere except for a finite number of nodes of the lattice. Having done that we study the bound states for the operator $H = H_0 + V$ using the Green's function associated with the operator H_0. The advantage of this method is that the Green's function on the lattice has a nice analytical representation which allows one to compute the eigenstates and eigenmodes with high accuracy. For alternative approaches on the computation of the eigenmodes using grid methods see [9] and references therein.

2. ONE-BAND MODEL

Let us consider the one-band model. The spectral properties of the propagation of electron, acoustic and electromagnetic waves in three-dimensional inhomogeneous media are reduced to the spectral properties of the operators

$$T_S\psi(x) = -\Delta\psi(x) + \tau(S,x)\psi(x) \tag{1}$$

$$T_A\psi(x) = -\nabla\tau^{-1}(A,x)\nabla\psi(x) \tag{2}$$

$$T_M\Psi(x) = -\nabla\times\tau^{-1}(M,x)\nabla\times\Psi(x), \quad \nabla\cdot\Psi(x) = 0, \tag{3}$$

where x is a point in three-dimensional space and $\tau(S, x)$, $\tau(A, x)$, $\tau(M, x)$ are the potential, position-dependent mass density, and dielectric constant, respectively. Let $\tau_0(x)$ be the function describing the underlying periodic medium. For simplicity we assume the elementary cell is just the unit cube and, hence, for any three component vector m with integer valued coordinates we have the equality

$$\tau_0(x+m) = \tau_0(x). \tag{4}$$

Then let the function $\tau(x)$ describe the periodic medium with a defect

$$\tau(x) = \tau_0(x) + \delta\tau(x), \tag{5}$$

where the perturbations $\delta\tau(x)$, called a defect, are assumed to vanish outside a bounded domain Λ. We assume that the spectrum of the operator T_0 associated with $\tau_0(x)$ has a gap (a, b) in the spectrum.

An eigenmode $u_\lambda(x)$ for $T = T_0 + \delta T$ associated with the eigenstate λ is considered to be bounded (localized) if

$$Tu_\lambda(x) = \lambda u_\lambda(x), \quad \int |u(x)|^2\, dx < \infty. \tag{6}$$

In the cases of the operators (1)–(3) if $u_\lambda(x)$ is bound it is usually exponentially bound, namely

$$u_\lambda(x) = \alpha_\lambda(x) \exp\left(-\frac{|x|}{L_\lambda}\right), \tag{7}$$

where $\alpha_\lambda(x)$ is at least bounded and, possibly, oscillating. We will refer to the number L_λ as the localization length of the eigenstate λ (impurity state).

One can study the properties of a bound eigenmode $u_\lambda(x)$ with the eigenstate λ in the gap (a, b) (see [10, 5, 6]) as follows: First, we rewrite Eq. (6) in the form

$$u_\lambda(x) = (\lambda - T_0)^{-1}\, \delta T u_\lambda(x) = \int G_0(\lambda; x, y)[\delta T u_\lambda](y)\, dy, \tag{8}$$

where $G_0(\lambda; x, y)$ is the Green's function for T_0. Note now that since λ is the gap of the spectrum for T_0 then for any of the operators T_0 of the form (1), (2), and (3) its Green's function $G_0(\lambda; x, y)$ decays exponentially as $|x - y|$ approaches infinity (see [10] for the Schrödinger operator, [11] for acoustic waves, and [12] for electromagnetic waves). Since the defect is confined in a bounded domain, then the formula (8) implies readily that $u_\lambda(x)$ decays exponentially with the rate of the decay of the Green's function $G_0(\lambda; x, y)$.

Since $\tau_0(x)$ is a periodic function, the following Bloch decomposition holds for the Green's function,

$$G_0(\lambda; x, y) = \sum_{n \geq 1} \int_K \frac{g_n(k, x) g_n^*(k, y)}{\lambda - \omega_n(k)}\, dk, \quad K = [0, 2\pi]^3, \tag{9}$$

where k is the Bloch quasimomentum, K is the Brillouin zone, $\omega_n(k)$ and $g_n(k)$ are respectively the Bloch eigenvalues and eigenmodes for T_0. Consider the nth spectral band $[b_n, a_n]$,

$$b_n = \min_{k \text{ in } K} \{\omega_n(k)\}, \quad a_n = \max_{k \text{ in } K} \{\omega_n(k)\} \tag{10}$$

and since λ is in a spectral gap we have for some n_0,

$$a_{n_0} = a < \lambda < b = b_{n_0+1}. \tag{11}$$

Assuming λ is closer to a we consider the most singular term in the sum (9),

$$\tilde{G}_0(\lambda; x, y) = \int_K \frac{g_{n_0}(k, x) g^*_{n_0}(k, y)}{\lambda - \omega_{n_0}(k)}\, dk, \tag{12}$$

associated with one band $[b_{n_0}, a_{n_0}]$ and the function $\omega_{n_0}(k)$. This term determines the basic properties of the u_λ in Eq. (8) [6], and hence, one can consider the following simpler operator instead of the original one:

$$H_0\psi(k) = \omega_{n_0}(k)\psi(k), \quad k \text{ in } K. \tag{13}$$

In view of its structure, it is natural to call H_0 from (13) *a one-band model.* If we denote by $\mathbb{Z}^3$ three-dimensional lattice, i.e. the set of integer-valued triplets $n = (n_1, n_2, n_3)$, then the operator H_0 defined by (13) after the Fourier transform $\psi_n = \int_K e^{-ikn}\psi(k)\, dk$ takes the form

$$[H_0\psi]_n = \sum_{m \text{ in } \mathbb{Z}^3} H_{0;n-m}\psi_n, \quad H_{0;n} = \int_K e^{-ikn}\omega_{n_0}(k)\, dk, \quad n \text{ in } \mathbb{Z}^3. \tag{14}$$

In particular, if we take for $H_0(k) = \omega_{n_0}(k)$ the simplest possible periodic function having one maximum and one minimum value with the form

$$-\Delta(k) = 2\sum_{j=1}^{3} (1 - \cos k_j) \tag{15}$$

then

$$[-\Delta]_n = = \begin{cases} 6 & \text{if } n = 0 \\ -1 & \text{if } |n_1| + |n_2| + |n_3| = 1 \\ 0 & \text{otherwise,} \end{cases} \tag{16}$$

and the operator $-\Delta$ will be the lattice version of Laplacian. Indeed, as follows from (14) and (16) we have

$$[-\Delta\psi]_n = \sum_{j=1}^{3} [\psi_n - \psi_{n+e_j}] + \sum_{j=1}^{3} [\psi_n - \psi_{n-e_j}], \quad n \text{ in } \mathbb{Z}^3. \tag{17}$$

Assuming now that the periodic medium is described by $-\Delta$ we introduce the defect as the potential V_Λ that vanishes outside of a given domain Λ in the lattice $\mathbb{Z}^3$. Hence, the medium with the defect is described by the operator $H = H_{V_\Lambda}$ and

$$[H\psi]_n = [(-\Delta + V_\Lambda)\psi]_n = -\Delta\psi_n + v_n\psi_n \tag{18}$$

$$V_\Lambda = \begin{cases} v_n & \text{if } n \text{ in } \Lambda \\ 0 & \text{otherwise.} \end{cases} \tag{19}$$

Note that the operator H defined by (18) is a known lattice model of the Schrödinger operator. The continuum version of the Schrödinger operator with a finite number of point defects was studied in [8]. Thus, we study bound eigenmodes and eigenstates of the operator H defined (18) as a typical example of one-band model.

In the sequel the symbol x will stand for the space point on the 3D lattice $\mathbb{Z}^3$.

3. EIGENMODES AND GREEN'S FUNCTIONS

We consider here the general approach for the representation of the bound states in terms of the Green's function for an unperturbed medium and its implementation for some cases of interest.

3.1. *General Case Representation*

Suppose that we have an operator $H = H_0 + V$, where H_0 has a gap (a, b) in the spectrum and the operator $V \leq 0$ is the sum of orthogonal projectors of the form

$$V = -\sum_{x \text{ in } \Lambda} v_x |f_x\rangle\langle f_x|, \quad v_x > 0, \tag{20}$$

where Λ is a finite set of indices and the vectors f_x form an orthonormal set of vectors, i.e. $(f_x, f_y) = \delta_{x,y}$, where $\delta_{x,y}$ is the Kronecker symbol. The case when $V \geq 0$ can be treated in a similar way. Suppose that H has an eigenvalue λ in the gap (a, b), and hence, for a vector ψ from $l_2(\mathbb{Z}^3)$ we have

$$H\psi = \lambda\psi, \tag{21}$$

or

$$H_0\psi - \sum_{x \text{ in } \Lambda} v_x f_x (f_x, \psi) = \lambda\psi. \tag{22}$$

Introducing now the resolvent operator $G_0(\lambda) = (H_0 - \lambda I)^{-1}$, which is merely the operator form of Green's function, we rewrite (22) as

$$\psi = \sum_{x \text{ in } \Lambda} v_x (f_x, \psi) G_0(\lambda) f_x. \tag{23}$$

Observe that Eq. (23) clearly implies that the eigenvector ψ is a linear combination of the vectors $G_0(\lambda) f_x$, namely

$$\psi = \sum_{x \text{ in } \Lambda} \beta_x G_0(\lambda) f_x. \tag{24}$$

To find the coefficients β_x we substitute (24) in (23) and get

$$\sum_{x \text{ in } \Lambda} \beta_x G_0(\lambda) f_x = \sum_{x,y \text{ in } \Lambda} \beta_y v_x (f_x, G_0(\lambda) f_y) R_0(\lambda) f_x, \tag{25}$$

or

$$\beta_x = \sum_{x,y \text{ in } \Lambda} \beta_y v_x (f_x, G_0(\lambda) f_y), \quad x \text{ in } \Lambda. \tag{26}$$

Let us introduce now the matrices

$$G_{0,\Lambda}(\lambda) = \{(f_x, G_0(\lambda) f_y), x, y \text{ in } \Lambda\}, \quad V_\Lambda = \{v_x \delta_{xy}, x, y \text{ in } \Lambda\}. \tag{27}$$

Note that both matrices $G_{0,\Lambda}(\lambda)$ and V_Λ are nonnegative and Hermitian and so problem (26) takes the form

$$\beta = V_\Lambda G_{0,\Lambda}(\lambda) \beta. \tag{28}$$

The latter is equivalent to the eigenvalue problem:

$$\zeta = \mathbf{G}_{V_\Lambda}(\lambda) \zeta, \quad \sqrt{V_\Lambda} \zeta = \beta, \tag{29}$$

$$\mathbf{G}_{V_\Lambda}(\lambda) = \{\sqrt{v_x v_y} (f_x, G_0(\lambda) f_y), x, y \text{ in } \Lambda\}. \tag{30}$$

Let us denote the eigenvalues and the eigenvectors of the Hermitian matrix $\mathbf{G}_{V_\Lambda}(\lambda)$, respectively, by $g_n(\lambda)$ and $\zeta_n(\lambda)$, $n = 1, ..., |\Lambda|$, where $|\Lambda|$ is the number of sites in the set Λ. Then the bound states λ_n of the original problem (21) are the solutions of the equations

$$g_n(\lambda) = 1, \quad n = 1, ..., |\Lambda|. \tag{31}$$

Having found λ_n from Eq. (31), we then find the corresponding vector β using (29)–(30) as follows:

$$\beta(\lambda_n) = \sqrt{V_\Lambda} \zeta_n(\lambda_n), \quad \beta_y(\lambda_n) = \sqrt{v_y} [\zeta_n(\lambda_n)]_y, \quad y \text{ in } \Lambda. \tag{32}$$

This equality, together with Eq. (24), gives the representation for the bound eigenmode $\varphi_{\lambda_n}(x)$ associated with the eigenvalue λ_n:

$$\varphi_{\lambda_n}(x) = \sum_{y \text{ in } \Lambda} \sqrt{v_y} [\zeta_n(\lambda_n)]_y (f_x, G_0(\lambda) f_y), \quad x \text{ in } \mathbb{Z}^3. \tag{33}$$

Summarizing, we find the bound states λ_n by solving Eqs. (31) and then we compute the corresponding eigenmodes $\varphi_{\lambda_n}(x)$ by solving the eigenvalue problem (29)–(30) and plugging its results into the representation (33).

It is evident that the Green's function $(f_x, G_0(\lambda) f_y)$ plays the central role in the method we use. For the case of 3D lattice Laplacian (17) the associated Green's function can be represented as

$$(f_y, G_0(\lambda) f_x) = G_0(\lambda; x - y), \qquad \lambda < 0 \tag{34}$$

$$G_0(\lambda; x) = \int_K \frac{\exp\{-2\pi i k x\}\, dk}{-\lambda + \sum_{j=1}^3 2(1 - \cos 2\pi k_j)}, \quad x \text{ in } \mathbb{Z}^3. \tag{35}$$

In Eq. (34) the vectors f_x form the standard basis in the Hilbert space $l_2(\mathbb{Z}^3)$ of the square summable sequences on the lattice $\mathbb{Z}^3$; i.e., $(f_x)_y = \delta_{xy}$.

The method is similar to one from [8] developed for the Schrödinger operator in the continuum with a finite number of point defects.

3.2. *Lattice Laplacian*

Let us begin with the case of a point defect $\Lambda = \{0\}$ when $v_x = v\delta_{x0}$. Using Eqs. (30), (34), and (35), we find that the matrix $\mathbf{G}_v(\lambda)$ is just a scalar and

$$\mathbf{G}_v(\lambda) = v \int_K \frac{dk}{-\lambda + \sum_{j=1}^3 2(1 - \cos 2\pi k_j)}, \quad \lambda < 0. \tag{36}$$

The equation of the localized (impurity) states (31) then has the form:

$$vg(\lambda) = 1, g(\lambda) = \int_K \frac{dk}{-\lambda + \sum_{j=1}^3 2(1 - \cos 2\pi k_j)}. \tag{37}$$

Note that $g(\lambda)$ for $\lambda < 0$ is an increasing function such that

$$\lim_{\lambda \to -0} g(\lambda) = g(0) = \int_K \frac{dk}{\sum_{j=1}^3 2(1 - \cos 2\pi k_j)} \tag{38}$$

$$\lim_{\lambda \to -0} \frac{[g(\lambda) - g(0)]}{\sqrt{-\lambda}} = -\int_{k \text{ in } \mathbb{R}^3} \frac{dk}{[1 + (2\pi k)^2](2\pi k)^2} = \frac{1}{4\pi} \tag{39}$$

$$g(\lambda) = g(0) - \frac{\sqrt{-\lambda}}{4\pi} + o(\sqrt{-\lambda}), \quad \lambda \to -0 \tag{40}$$

$$g(\lambda) = -\lambda^{-1} + \int_K \frac{\sum_{j=1}^3 2(1 - \cos 2\pi k_j)\, dk}{-\lambda[-\lambda + \sum_{j=1}^3 2(1 - \cos 2\pi k_j)]} \tag{41}$$

$$= -\lambda^{-1} + O(\lambda^{-2}), \quad \lambda \to -\infty. \tag{42}$$

If $\lambda(v)$ is a solution to (37) then the corresponding bound eigenfunction is

$$\varphi_{\lambda(v)}(x) = \int_K \frac{\exp\{-2\pi i k x\}\, dk}{-\lambda(v) + \sum_{j=1}^3 2(1 - \cos 2\pi k_j)}, \quad x \text{ in } \mathbb{Z}^3. \tag{43}$$

For a more general V of the form (20), where the number of defects can be arbitrary, we have

$$\mathbf{G}_V(\lambda; x, y) = \sqrt{v_x v_y} G_0(\lambda; x - y), \quad x, y \text{ in } \Lambda, \tag{44}$$

$$G_0(\lambda; x) = \int_K \frac{\exp\{-2\pi i k x\}\, dk}{-\lambda + \sum_{j=1}^3 2(1 - \cos 2\pi k_j)}, \quad x \text{ in } \mathbb{Z}^3. \tag{45}$$

Then the bound states and eigenmodes can be found using (31)–(33).

4. GREEN'S FUNCTION COMPUTATION

In this section we consider some basic properties of the Green's function of the 3D lattice Laplacian which will be needed for the computation of the bound states and eigenmodes. The Green's function defined by the integral (45), unlike the Green's function of the Laplacian in the 3D continuum, is not explicitly reducible to an elementary or a special function. In the next subsection we describe a numerically efficient representation for the integral (45) for some range of negative λ. To verify the accuracy of the representations we consider the following identities for the Green's function. First note that, based on (17), we have $(-\Delta - \lambda)G_0(\lambda; x) = \delta_{x0}$ and, hence,

$$(6 - \lambda)G_0(\lambda; x) - \sum_{j=1}^{3} [G_0(\lambda; x + e_j) + G_0(\lambda; x - e_j)] = \delta_{x0}, \quad x \text{ in } \mathbb{Z}^d. \tag{46}$$

In addition, from (45) it follows that

$$G_0(\lambda; \pm e_1) = G_0(\lambda; \pm e_2) = G_0(\lambda; \pm e_3) = g_1(\lambda). \tag{47}$$

The latter, together with (46), implies for $x = 0$ that

$$(6 - \lambda)G_0(\lambda; 0) - \sum_{j=1}^{3} [G_0(\lambda; x + e_j) + G_0(\lambda; x - e_j)] = 1 \tag{48}$$

which gives

$$6g_1(\lambda) = (6 - \lambda)g(\lambda) - 1. \tag{49}$$

The identities (46)–(49) are also used to lessen the computations of $G_0(\lambda, x)$ for different values of x.

4.1. *Evaluation of the Green's Function*

Using the equality $1/F = \int_0^\infty \exp(-\rho F)\, d\rho$ we get the representation for the integral (45).

$$G_0(\lambda; x) = \frac{1}{4}\int_0^\infty d\rho \int_{[0,1]^3} \exp(\rho\mu) \exp\{-2\pi i k x\} \exp\left\{-\rho \sum_{j=1}^{3} \sin^2(\pi k_j)\right\} d^3k, \tag{50}$$

where $\mu = \lambda/4 < 0$. After elementary transformations we obtain

$$G_0(\mu; x) = \frac{1}{4}\int_0^\infty A_\rho(x_1)A_\rho(x_2)A_\rho(x_3)\exp\{\mu\rho\}\, d\rho \tag{51}$$

$$A_\rho(x_i) = \int_0^1 \cos(2\pi k_i x_i) \exp\{-\rho \sin^2(\pi k_i)\}\, dk_i. \tag{52}$$

Taking into account that x_i are integers and evaluating integrals (52), we get the serial representation for the Green's function (further, we use this formula for the numerical computations),

$$G_0(\lambda; x) = (-\lambda + 6)^{-(r_1+r_2+r_3+1)} \sum_{j=0}^{\infty} (-\lambda + 6)^{-2j} R_j(r_1, r_2, r_3), \tag{53}$$

$$R_j(r_1, r_2, r_3) = \sum_{j_1+j_2+j_3=j} \frac{(r_1 + r_2 + r_3 + 2j)!}{j_1!j_2!j_3!(r_1 + j_1)!(r_2 + j_2)!(r_3 + j_3)!}, \tag{54}$$

where $r_i = |x_i|$. In fact, the terms R_j can be interpreted as the probability to reach the site x from the origin in j steps for the Bernoulli random walk on the lattice.

The accuracy of the Green's function computation has been verified as follows. We have taken in the series (53) up to 50 terms, i.e. $0 \le j \le 50$, and have found that Eq. (46) holds with the error less than 10^{-3} for $\frac{1}{2} \le |\lambda| \le 1$, less than 10^{-4} for $1 \le |\lambda| \le 6$ and less than 10^{-6} for $|\lambda| > 10$.

4.2. *Green's Function Exponential Decay and Anisotropy*

Recall that the Green's function $G_0(\lambda; x)$ for $\lambda < 0$ is a nonnegative function, and hence, we may consider its Laplace transform

$$\hat{G}_0(\lambda; p) = \sum_x e^{px} G_0(\lambda; x), \quad \lambda < 0, \tag{55}$$

where

$$\hat{G}_0(\lambda; p) = \frac{1}{-\lambda + 2\sum_{j=1}^{d} (1 - \cosh p_j)}.$$

To describe the rate of the exponential decay of $G_0(\lambda; x)$ we introduce the set P_λ consisting of (p_1, p_2, p_3) with nonnegative p_j and having as its boundary the following surface:

$$-\lambda + 2 \sum_{j=1}^{d} (1 - \cosh p_j) = 0. \tag{56}$$

Then we have

$$G_0(\lambda; x) \le \min_{p \text{ in } P_\lambda} [\hat{G}_0(\lambda; p)] \exp\{-\max_{p \text{ in } P_\lambda} [px]\}. \tag{57}$$

The lattice Green's function $G_0(\lambda; x)$ is anisotropic. The spatial anisotropy of $G_0(\lambda; x)$ is especially pronounced in the case of large $|\lambda|$. This is illustrated on Fig. 1, where we present the boundaries of the sets P_λ defined by Eq. (56) for the cases of $|\lambda| = 100$ (Fig. 1a) and $|\lambda| = 2$ (Fig. 1b).

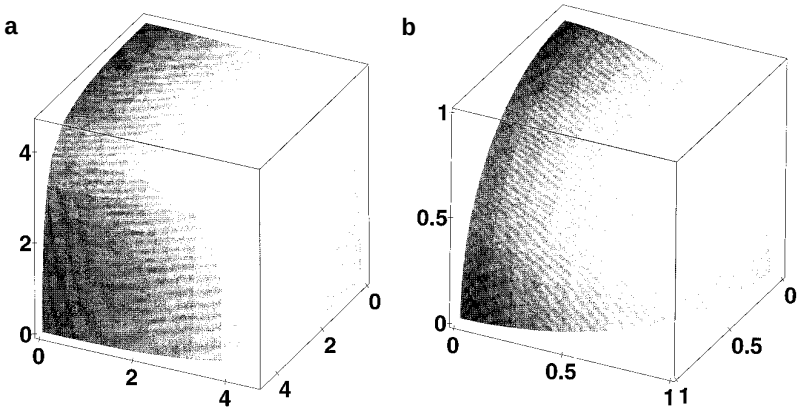

FIG. 1. Isosurface: the boundary of the set P_λ for $\lambda = 100$ (a) and $\lambda = 2$ (b).

5. COMPUTATION ALGORITHM

We wrote the FORTRAN program for the numerical solution of eigenvalue problem for 3D discrete Schrödinger operator on the lattice. Here we describe the algorithm.

Step 1. Data input. The program allows the date to be entered from a terminal or a read from a file. The data is stored as a matrix where each row corresponds to a defect and the columns represent the potential and the defect coordinates.

Step 2. For a given spatial configuration of the defects we evaluate the array of coefficients for the expansion of the Greens' function (see (54) and (53)). Since these coefficients are determined only by the geometry of the defect we keep the array in RAM to avoid repeated computations while changing options.

Step 3. Diagonalizing the matrix of Greens' functions and sorting its eigenvalues at $\lambda = 0$ we determine how many eigenstates the system has, i.e. how many eigenvalues of this matrix are greater than 0 (see (31) and (32)). This step determines the dimension of the array in which we store the eigenvalues and the eigenvectors of our problem.

Step 4. Starting from the point $\lambda = 0$ with an appropriately chosen step with respect to λ we find the value of λ which is the solution of Eq. (31). Then we diagonalize the matrix and sort only the eigenvalues which are greater or equal to 1. In particular, we solve Eqs. (31) and (32) and store the results in the array prepared during Step 3. We have also provided an additional option to evaluate and plot the characteristic polynomial of the matrix (44). Sometimes it is necessary to check the accuracy of diagonalization.

Step 5. After the previous step the eigenstates and the eigenmodes have been evaluated for the given set of defects. Now we can use different output options: 3D plot, different projections, and color maps. To scale the potential profile one should enter the scaling factor and go back to Step 3. To change the configuration of the defects one has to go to Step 1.

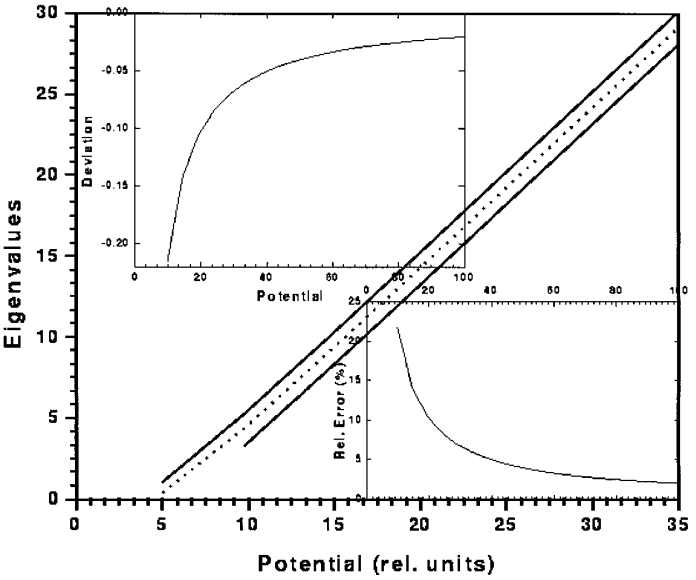

FIG. 2. The eigenvalues for two similar defects (solid lines), $x = 1$, and single defect (dashed line) vs potential. The upper inset shows the deviation (asymmetry) of the splitting, and the lower insert shows the relative error of the perturbation theory (first order) in comparison with the numerical computations.

Complete evaluation of the eigenvalue problem for four point defects takes approximately 1 min on the SUN SPARC Station-20, and approximately 1.5 h for 100 defects.

6. BOUND STATES AND EIGENMODES FOR SOME DEFECTS

In this section we describe the results of the computation of the eigenmodes and eigenstates for some arrangements of defects.

6.1. *The Case of Two Defects*

It is well known that the interaction of two defects leads to the splitting of energy levels. For the similar defects (2-well potential) the first order of the perturbation theory gives for the eigenstates $\lambda_{1,2}$,

$$\lambda_{1,2} = \lambda_0 \pm E(x), \tag{58}$$

where λ_0 is eigenvalue for the single defect, and $E(x)$ is the tunneling matrix element for two potential wells separated by the vector x, i.e. the interaction between the defects (see, for example, [13]). In fact, the splitting of eigenstates is not symmetric with respect to λ_0 because it is determined by both $G_0(\lambda; x)$ and $G_0(\lambda; 0)$ which have different slopes as functions of λ (see Eqs. (29)–(32)). Comparison of our numeric computations with the classical perturbation theory is presented in Fig. 2.

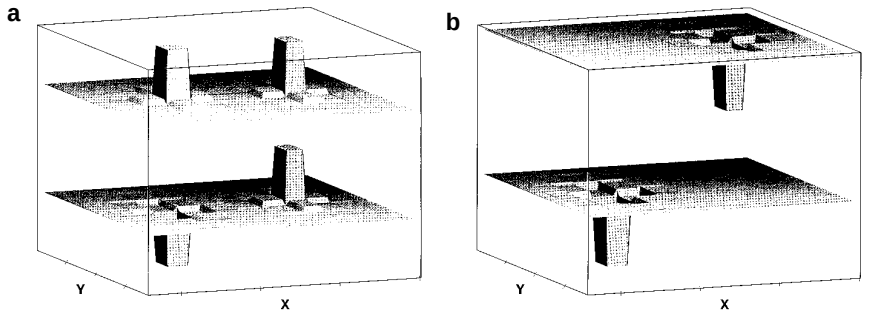

FIG. 3. The eigenfunctions for two defects with interdefect distance $|x| = 5$ and (a) equal potentials, $|v_1| = |v_2| = 10$; (b) different potentials $|v_1| = 10$, $|v_2| = 9.5$. In the case of assymetric potential (b) each of the eigenfunctions is well localized about only one of the two wells.

As one expects, for large eigenvalues the perturbation theory gives quite accurate results, but for small λ the relative error is rather large; in the considered case it is up to 20%. For two similar point defects (2-level system) the eigenfunctions corresponding to the ground state are symmetric and the eigenfunctions corresponding to the shallow state are antisymmetric. Both eigenfunctions are equally localized on both defects. In the case of even a relatively small asymmetry of the potential the geometry the eigenfunctions changes substantially; namely, one of the eigenmodes is more pronounced over one defect and another eigenmode is more pronounced over another defect. This effect becomes stronger with the increase of the distance between the defects. Figure 3 shows the eigenfunctions for two spatially separated defects with the interdefect distance $|x| = 5$. Figure 4 displays the eigenfunctions for two closely placed defects with the interdefect distance $|x| = 1$. Comparison of these plots shows that for small interdefect distances the eigenfunctions have a weak tendency for decoupling, while for the large distances the eigenfunctions decouple even for the small asymmetry of potentials, 5% in the considered case.

This well-known phenomenon was verified here as follows. We introduce for a

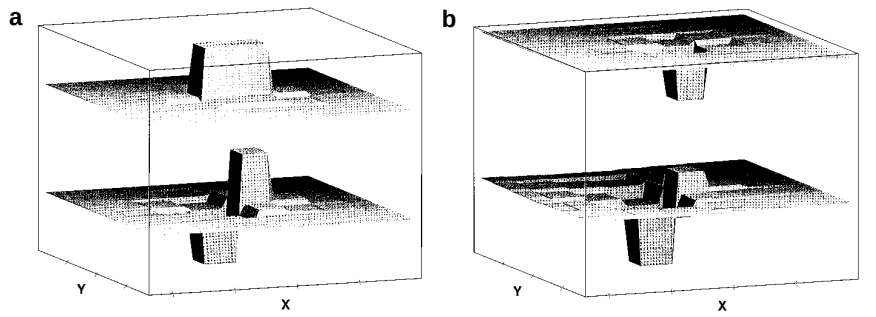

FIG. 4. The eigenfunctions for two defects with interdefect distance $|x| = 1$ and (a) equal potentials, $|v_1| = |v_2| = 10$; (b) significantly different potentials, $|v_1| = 10$, $|v_2| = 5$. In the case of assymetric potential (b) each of the eigenfunctions is well localized about only one of the two wells.

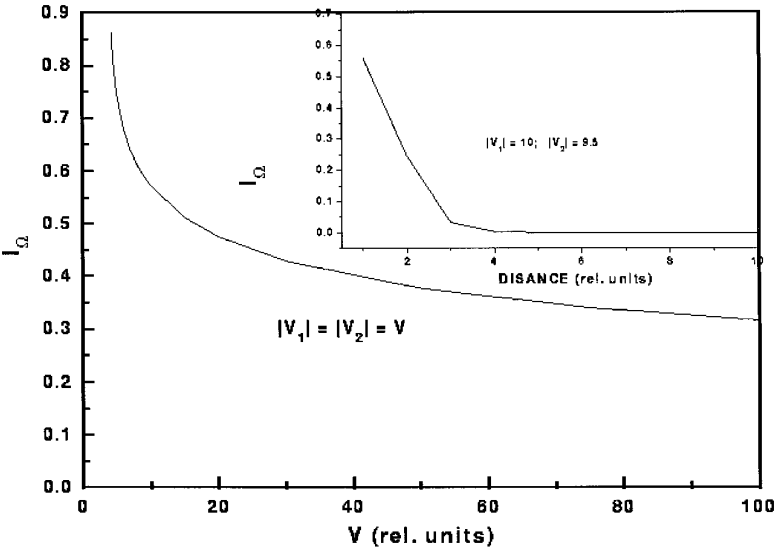

FIG. 5. The overlap integral versus potential. Inset shows the integral for fixed potentials $|v_1| = 10$, $|v_2| = 9.5$ versus the interdefect distance.

domain Ω the overlap integral for the normalized eigenfunctions $\varphi_{\lambda i}(x)$ and $\varphi_{\lambda j}(x)$ in the form

$$I_\Omega = \sum_{x \text{ in } \Omega} |\varphi_{\lambda i}(x)|\,|\varphi_{\lambda j}(x)|. \tag{59}$$

Since the localization radius grows when λ approaches 0, one can expect the increase of I_Ω with the decrease of the interdefect distance and the decrease of the potential. These results are presented in Fig. 5. It is clear, that integral (59) has a maximum when the potentials of the defects are equal. This integral also grows with the decrease of the potential, and in this case the eigenvalue decreases and the corresponding eigenfunction becomes delocalized. Dependence of I_Ω versus the potential of one defect when the second potential is constant is shown on Fig. 6. Here we can see the narrow maximum for equal potentials and the growth of the overlap integral for the potential approaching the critical value when the eigenstate appears.

6.2. *The Localization Radius*

As follows from formula (33) a bound eigenmode is a linear combination of some shifts of the Green's function, and the eigenmode also decays exponentially. We carried out the computation of the localization radius for the bound states which is defined as the coefficient L_λ in the representation of the eigenmode u_λ by formula (7). More precisely, we define L_λ by the relationship

$$-\liminf_{|x|\to\infty} \frac{\ln(|\varphi_\lambda(x)|)}{|x|} = \frac{1}{L_\lambda}. \tag{60}$$

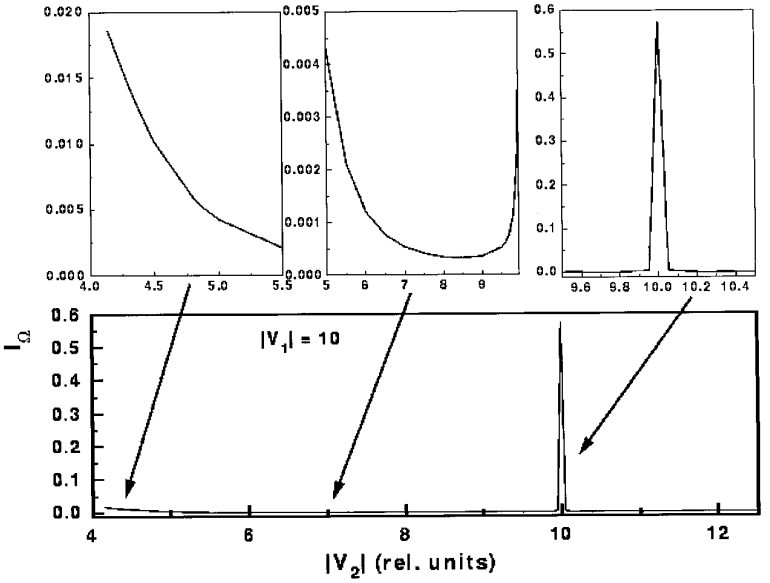

FIG. 6. Overlap integral vs potential of the second defect. Interdefect distance $x = 5$, potential of the first defect $|v_1| = 10$. Insets show peculiarities of I_Ω.

As is shown in [14], the localization radius for a single defect can be estimated by $L_\lambda \sim \sqrt{D(\lambda)}$ for small $D(\lambda)$, where $D(\lambda)$ is the distance from the bound state λ to the continuous spectrum, and this type of the dependence of L_λ on $D(\lambda)$ is considered to be universal for a wide class of physical systems.

We observe this dependence. In addition to that, since the Green's function is anisotropic so is the eigenmode $\varphi_\lambda(x)$. The latter implies that L_λ for the impurity state depends on the direction of x. On Fig. 7 and Fig. 8 we present the dependence of the eigenfunctions for the shallow level and the localization radius for the cases of one defect and four defects. These figures, together with Fig. 1, display strong anisotropy of the localization radius, especially with the increase of λ. These results also match the growth of I_Ω at the boundary of the gap shown in Fig. 5 and Fig. 6.

6.3. *Cubic Defect with a Cavity*

As an example we have evaluated the eigenvalues for a set of 26 site defects forming a cube of side 3 with a cubic cavity. The geometry of this configuration is shown in Fig. 9. The eigenvalues for the different potentials on the sites of defects are displayed in Table I, where all potential values on the defect sites are chosen to be equal, i.e. $v_1 = \cdots = v_{26} = v$.

7. CONCLUSIONS

We introduced and described a one-band model for bound states generated by impurities in a periodic medium and, as an example, carried out the computations

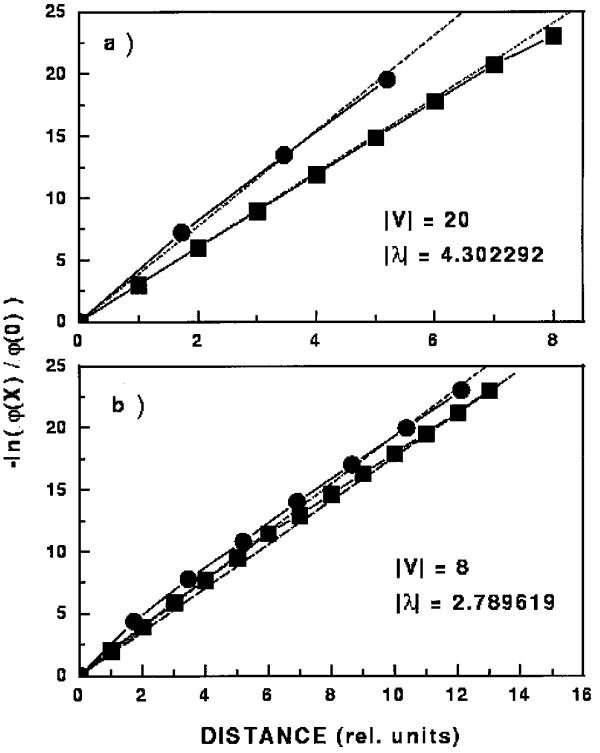

FIG. 7. The decay of the shallow eigenfunction for one defect versus distance in the directions [111] (circles) and [100] (squares), for the large potential, $|V| = 20$, (a), and small potential, $|V| = 8$, (b). Dotted and dashed lines show the dependence from (60).

for a 3D lattice Laplacian perturbed by a finite number of point defects. Using a Green's function method we achieve high accuracy in the computation of the eigenmodes and eigenstates for a variety of defects. We show the increase of the overlap integral for the shallow levels. We also computed the localization radius and its anisotropy for a given bound eigenmodes. For an appropriately chosen model these computations can be useful for the numerical estimates of the minimal defects capable of introducing a bound state in a gap, as well as for the computation of the rate of the exponential decay of the bound state.

Our model is verified by the qualitatively known behavior of the bound eigenmodes, such as the tunneling and the space anisotropy for the case of two remote defects.

ACKNOWLEDGMENTS AND DISCLAIMER

The efforts of A. Figotin and I. Khalfin are sponsored by the Air Force Office of Scientific Research, Air Force Materials Command, USAF, under Grant F49620-94-1-0172. The U.S. Government's right to retain a nonexclusive royalty-free license in and to the copyright covering this paper, for governmental purposes, is acknowledged. The views and conclusions contained herein are those of the authors and should not be interpreted as necessarily representing the official policies or endorsements, either expressed or implied, of the Air Force Office of Scientific Research or the U.S. Government. The authors are thankful to S. Molchanov for useful discussions.

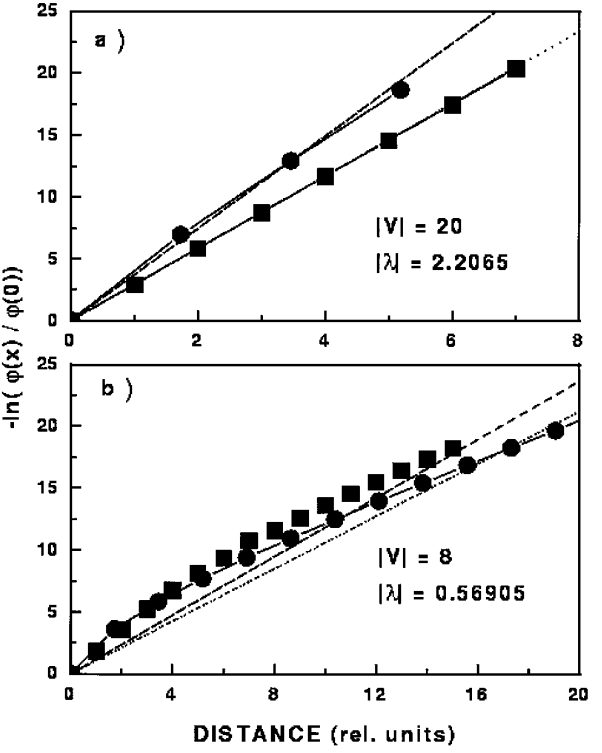

FIG. 8. Decay of the shallow eigenfunction for four defects versus distance in the directions [111] (circles) and [100] (squares), for the large potential, $|V| = 20$, (a); and small potential, $|V| = 8$, (b). Dotted and dashed lines show the dependence from (60).

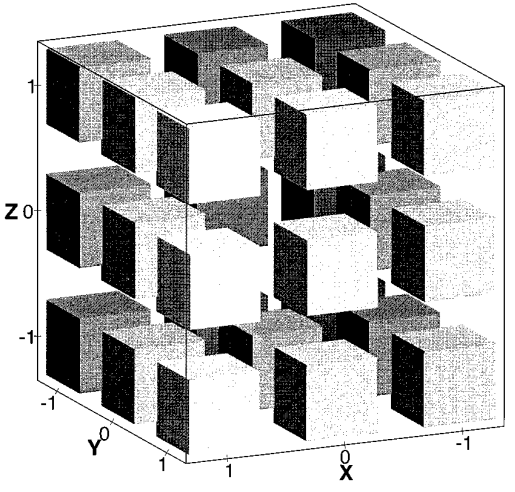

FIG. 9. Spatial configuration of the site defects forming a cube with an internal cubic cavity.

TABLE I

The Eigenvalues Are Given in Ascending Order Starting from the Ground State for 26 Sites Defect Forming a Cube with a Cubic Cavity (See Fig. 9) and a Set of Potentials $v = 5$, 7.5, 10, and 20 ($v_1 = \cdots = v_{26} = v$)

#	$v = 5$	$v = 7.5$	$v = 10$	$v = 20$
1	-3.257318	-3.247256	-8.043392	-17.906784
2	-2.203096	-3.247256	-7.019599	-16.925827
3	-2.203096	-3.247256	-7.019599	-16.925827
4	-2.203096	-3.112246	-7.019599	-16.925827
5	-0.972196	-3.112246	-5.662563	-15.538253
6	-0.972196	-2.113298	-5.662563	-15.538253
7	-0.972196	-1.916433	-5.662563	-15.538253
8	-0.722717	-1.781705	-5.561796	-15.488144
9	-0.722717	-1.781705	-5.561796	-15.488144
10		-1.781705	-4.463237	-14.234492
11		-1.777863	-4.306471	-14.150764
12		-1.777863	-4.205634	-14.100643
13		-1.777863	-4.205634	-14.100643
14		-1.777863	-4.205634	-14.100643
15		-0.449176	-4.204362	-14.100510
16		-0.449176	-4.204362	-14.100510
17		-0.449176	-4.204362	-14.100510
18		-0.449176	-2.848561	-12.713027
19		-0.449176	-2.848561	-12.713027
20		-0.449176	-2.848561	-12.713027
21		-0.310906	-2.746996	-12.662877
22		-0.310906	-2.746996	-12.662877
23			-1.390867	-11.275335
24			-1.390867	-11.275335
25			-1.390867	-11.275335
26			-0.709519	-10.460519

REFERENCES

1. S. John, *Phys. Today,* **May,** 32 (1991).
2. C. M. Soukoulis (Ed.), *Photonic Band Gaps and Localization,* NATO ASI Series B: Physics, Vol. 308 (Plenum, New York, 1993).
3. P. Sheng (Ed.), *Scattering and Localization of Classical Waves* (World Scientific, Singapore, 1990).
4. N. W. Ashcroft and N. D. Mermin, *Solid State Physics* (Holt, Rinehart, & Winston, New York/London, 1976).
5. A. Figotin and A. Klein, Localized classical waves created by defects, *J. Statist. Phys.* **86,** 165 (1997).
6. A. Figotin and A. Klein, Midgap defect modes in dielectric and acoustic media, *SIAM J. Appl. Math.,* to appear.
7. L. I. Schiff, *Quantum Mechanics* (McGraw–Hill, New York, 1965).
8. S. Albeverio, F. Gesztesy, R. Høegh-Krohn, and H. Holden, *Solvable Models in Quantum Mechanics,* Text and Monographs in Physics (Springer-Verlag, New York/Berlin, 1988).
9. M. Braun, S. A. Sofianos, D. G. Papageorgio, and I. E. Lagaris, *J. Comput. Phys.* **126,** 315 (1996).
10. M. Reed and B. Simon, Analysis of operators, in *Methods of Modern Mathematical Physics,* Vol. IV, (Academic Press, New York/London, 1978).
11. A. Figotin and A. Klein, Localization of classical waves I. Acoustic waves, *Commun. Math. Phys.* **180,** 439 (1996).
12. A. Figotin and A. Klein, *Localization of classical waves II. Electromagnetic waves,* in *Commun. Math. Phys.* **184,** 411 (1997).
13. L. D. Landau and E. M. Lifshitz, *Quantum Mechanics: Non-Relativistic Theory,* 3d ed. (Pergamon, Oxford/New York, 1977).
14. F. Martinelli and E. Scoppola, *Rivista Nuovo Cimento* **10,** N10 (1987).